OXFORD

Antibody Therapeutics, 2024, 7(3), 209–220
https://doi.org/10.1093/abt/tbae017
Advance access publication date 21 June 2024
Research Article

Fc engineering by monoclonal mammalian cell display for improved affinity and selectivity towards FcγRs

Zening Wang[1,2], Minhyo Kang[2], Afshin Ebrahimpour[1], Chuan Chen[2], Xin Ge[1,2,*]

[1]Institute of Molecular Medicine, University of Texas Health Science Center at Houston, 1825 Pressler St, Houston, TX 77030, United States
[2]Department of Chemical and Environmental Engineering, University of California Riverside, 900 University Ave, Reverside, CA 92521, United States

*Corresponding author. E-mail: xin.ge@uth.tmc.edu

Abstract

Fc optimization can significantly enhance therapeutic efficacy of monoclonal antibodies. However, existing Fc engineering approaches are sub-optimal with noted limitations, such as inappropriate glycosylation, polyclonal libraries, and utilizing fragment but not full-length IgG display. Applying cell cycle arrested recombinase-mediated cassette exchange, this study constructed high-quality monoclonal Fc libraries in CHO cells, displayed full-length IgG on cell surface, and preformed ratiometric fluorescence activated cell sorting (FACS) with the antigen and individual FcγRs. Identified Fc variants were quantitatively evaluated by flow cytometry, ELISA, kinetic and steady-state binding affinity measurements, and cytotoxicity assays. An error-prone Fc library focusing on the hinge-C_H2 region was constructed in CHO cells with a functional diversity of 7.5×10^6. Panels of novel Fc variants with enhanced affinity and selectivity for FcγRs were isolated. Particularly, clone 2a-10 (G236E/K288R/K290W/K320M) showed increased binding strength towards FcγRIIa-131R and 131H allotypes with kinetic dissociation constants ($K_{D\text{-}K}$) of 140 nM and 220 nM, respectively, while reduced binding strength towards FcγRIIb compared to WT Fc; clone 2b-1 (K222I/V302E/L328F/K334E) had $K_{D\text{-}K}$ of 180 nM towards FcγRIIb; clone 3a-2 (P247L/K248E/K334I) exhibited $K_{D\text{-}K}$ of 190 nM and 100 nM towards FcγRIIIa-176F and 176 V allotypes, respectively, and improved potency of 2.0 ng/ml in ADCC assays. Key mutation hotspots were identified, including P247 for FcγRIIIa, K290 for FcγRIIa, and K334 for FcγRIIb bindings. Discovery of Fc variants with enhanced affinity and selectivity towards individual FcγR and the identification of novel mutation hotspots provide valuable insights for further Fc optimization and serve as a foundation for advancing antibody therapeutics development.

Statement of Significance
Fc optimization is critical in improving therapeutic efficacy, but current engineering methods have limitations. By constructing large monoclonal mutagenesis libraries and displaying full-length IgG on CHO cells, novel Fc variants with enhanced affinity and selectivity for individual FcγRs were isolated and validated by multiple measurements and cytotoxicity assays.

Keywords: Fc engineering; mammalian cell display; RMCE; FcγR; ADCC

Introduction

Monoclonal antibodies (mAbs) have proven to be remarkably versatile therapeutics for the treatment of autoimmune, infectious, and malignant diseases [1–4]. Their efficacy stems not only from the antigen-specific Fab fragments but also from the Fc domain (IgG1 isotype in most cases), which activates complement and modulates effector functions through interaction with Fc gamma receptors (FcγRs) presenting on a variety of immune cells. Especially, the low affinity activating receptors FcγRIIIa and FcγRIIa are the main contributors to antibody-dependent cell-mediated cytotoxicity (ADCC) and antibody-dependent cell-mediated phagocytosis (ADCP) [5, 6], respectively. In consequence, antibodies with improved affinities towards FcγRIIIa or FcγRIIa exhibit enhanced ADCC or ADCP, leading to better efficacy in cancer and antiviral treatments [7–10]. Polymorphism on human FcγRs also highlights the clinical importance of antibody-FcγR binding strength. For example, anti-CD20 mAb rituximab performs better in lymphoma patients carrying FcγRIIIa-176 V than the 176F allotype, which correlates with observations that the 176 V allotype binds IgG1 Fc stronger [11–14]. Similarly, FcγRIIa-131R allotype is associated with greater susceptibility to infectious diseases due to its lower affinity to IgG1 Fc compared to FcγRIIa-131H [15–17]. In addition, interactions between Fc and inhibitory receptor FcγRIIb are crucial for the antitumor activity of agonistic mAbs [18–20].

Given the critical role of Fc-FcγR interactions in antibody-mediated effector functions, numerous strategies have been exploited to optimize Fc sequences for enhanced engagements with FcγRs. By computational designs, Fc mutant DEL (S239D/I332E/A330L) was identified showing a 58-fold increased affinity towards FcγRIIIa-176F compared to wild type (WT) trastuzumab [21]. Further screening more than 900 variants yielded Fc clones GA (G236A) and GAALIE (G236A/I332E/A330L) that demonstrated up to 6-fold improvement of binding to

Received: February 13, 2024. **Revised:** May 29, 2024. **Accepted:** June 20, 2024

FcγRIIa-131R [17]. Likewise, comprehensive mutagenesis studies discovered clones PD (P238D) and V12 (E233D/G237D/P238D/H268D/P271G/A330R) with improved binding selectivity towards FcγRIIb [22]. Despite largely successful, these site-directed mutagenesis approaches are often constrained to known FcγR epitopes, overlooking remote but potentially valuable mutation positions. To overcome this limitation, directed evolution has also been employed to isolate function-enhanced Fc variants [23, 24]. Screening from yeast surface displayed random mutagenesis libraries discovered Fc clone LPL (F243L/R293P/Y300L) with a 4.6-fold reduction in off-rate binding constant (k_{off}) and clone LPLIL (F243L/R292P/Y300L/V305I/P396L) with a > 10-fold lower dissociation constant (K_D), both towards FcγRIIIa-176F [25]. Furthermore, the construction of aglycosylated Fc libraries for periplasmic display in *E. coli* led to the isolation of Fc variants with improved bindings to individual FcγRs, including Ia [26], IIa [27], and IIIa [28]. Additionally, Fc variants with abolished FcγR engaged effector functions have also been isolated by *E. coli* periplasmic display [29].

A notable challenge of using microbes for Fc engineering is glycosylation. It has been well established that N-glycosylation at Asn297 of the Fc region is critical for effective FcγR recognition [30, 31]. In this context, mammalian cell systems are attractive platforms by ensuring proper protein folding and correct post-translational modifications. Accordingly, episomal transfection and lentiviral transduction have been applied for Fc optimization [32, 33]. However, these combinatorial library construction approaches are suboptimal with issues including low diversity, transgene instability, and multiple variants per cell (*i.e.*, polyclonality), which complicates the downstream clone identification. To address those issues, we recently developed cell cycle arrested recombinase-mediated cassette exchange (aRMCE) [34], allowing for construction of large and high-fidelity combinatorial libraries in mammalian cells with each transgene integrated to the same genomic location in a single copy per cell manner. Applying aRMCE, $>10^7$ diversity Fc mutagenesis libraries have been constructed and fully validated by deep sequencing, from which a few representative Fc mutants with improved affinity and selectivity towards FcγRs were identified and characterized [34]. In this follow-up study, we verified that aRMCE-mediated full-length IgG display on CHO cells enabled fine differentiation of Fc variants based on their affinities towards FcγRIIIa, FcγRIIa, and FcγRIIb. We further detailed how a comprehensive workflow for efficient Fc engineering was established, including magnetic-activated cell sorting (MACS), radiometric FACS, monoclonal flow cytometry screening, and ELISA. Apart from our previous work, multifaceted evaluations were reported in the current study, *e.g.*, both binding kinetics and steady-state equilibrium measurements. Additionally, in total 53 Fc variants were assayed, and top five clones were tested for ADCC with a new target cell line. Collectively, all these new data demonstrated the successful isolation of panels of Fc variants with improved affinity, selectivity, and efficacy.

Results

Monoclonal Fc mutagenesis library construction in CHO cells via high-efficient aRMCE

Recombinase-mediated cassette exchange (RMCE) is a DNA recombination event occurring at sequence-defined sites between a donor plasmid and a transgenic 'landing pad' on the chromosome [35, 36]. With a single landing pad at a locus of optimal target gene expression, both monoclonality and uniformed high transcription level can be achieved. In our previous work, a monoclonal cell line CHO-puro-3f8LC (clone 8) was generated [34], which harbors a single landing pad of *FRT* and *loxP* recognition sites and a 3f8 IgG (anti-TNFα antibody) light chain expression cassette on its genome (Fig. 1A). Co-transfection of this cell line with an expression plasmid encoding recombinases *Flp* and *Cre* and a promoter-less donor plasmid encoding 3f8 heavy chain leads to genomic integration of the heavy chain gene and display of full-length 3f8 IgG on the cell surface (Fig. 1A), facile for flow cytometry analysis of IgG expression and FcγR binding simultaneously. Importantly, applying nocodazole treatment during transfection results in improved RMCE efficiency, likely due to cell cycle arrested at the early mitosis phase, in which the integrity of nuclear membrane, a barrier for DNA transportation, is temporarily compromised [34].

Using this approach of cell cycle aRMCE, CHO-puro-3f8LC cells were transfected with 3f8 heavy chain donor plasmid encoding WT Fc, and the IgG display was detected with anti-IgG-PE (Fig. 1A). Flow cytometry analysis revealed that, without antibiotic selection, 18.9% of transfected cells were IgG positive (Fig. 1B). This high efficiency of genomic integration and IgG display were also observed for aRMCE transfections with 3f8 heavy chain carrying Fc variants LPL [25] and DEL [21]—resulted in 17.3% and 11.6% IgG positive cells, respectively. However, other tested Fc variants, including GA [17], GAALIE [17], PD [22], and V12 [22], showed 3–6% IgG positive populations (Fig. 1B). Given that the same aRMCE procedure was used, these reduced IgG displays were presumably caused by impacts of these Fc mutations on IgG synthesis, assembly, and/or translocation to cellular membrane. To generate Fc mutants with enhanced binding affinities towards FcγRs, random mutagenesis was introduced by error-prone PCR (EP-PCR) at human IgG1 hinge-C_H2 region (Fig. 2A), which contains FcγR epitopes [23, 37], and 1.5×10^8 *E.coli* transformants were obtained [34]. Under nocodazole treatment, 3×10^8 CHO-puro-3f8LC cells were transfected with the Fc mutagenesis library plasmids. Flow cytometry analysis showed that 2.5% of transfected cells displayed IgG (Fig. 1B), indicating a functional library size of 7.5×10^6, a diversity consistent with deep sequencing results and statistical estimation [34].

Isolation of Fc variants with improved binding towards specific FcγRs

To mimic the event of effector cell recruitment and to eliminate the disparity on display levels among Fc variants, a ratiometric flow cytometry approach was used, in which antigen recognition was monitored with EGFP-TNFα, and bindings to individual biotin-FcγRs were detected with streptavidin-APC (Fig. 2A). When tested on CHO cells displaying IgG encoding WT or mutated Fc, flow cytometry analysis indicated that compared to Fc WT, the cell populations of DEL and LPL clones tilted significantly towards FcγRIIIa-176F binding (Fig. 2B), consistent with their improved affinities [21]. Towards FcγRIIa, Fc clones GA and GAALIE also exhibited expected rightward tilts on their plots, with 0.33% and 0.059% $FcγRIIa^{high}$ cells, respectively (Fig. 2B). Despite <2-fold difference between their K_D values, *i.e.*, 488 vs 819 nM [17], the ratiometric flow cytometry successfully distinguished these two clones. Similarly, 7.39% of clone V12 cells were $FcγRIIb^{High}$ (Fig. 2B), a dramatic increase compared to the value of 0.03% for clone PD, reflecting the 62-fold affinity enhancement between them [25]. Collectively, above results suggested that CHO cell IgG display followed by the ratiometric flow cytometry is a reliable method to distinct Fc clones of different affinities towards FcγR targets, and thus ready for isolation of Fc variants from mutagenesis libraries.

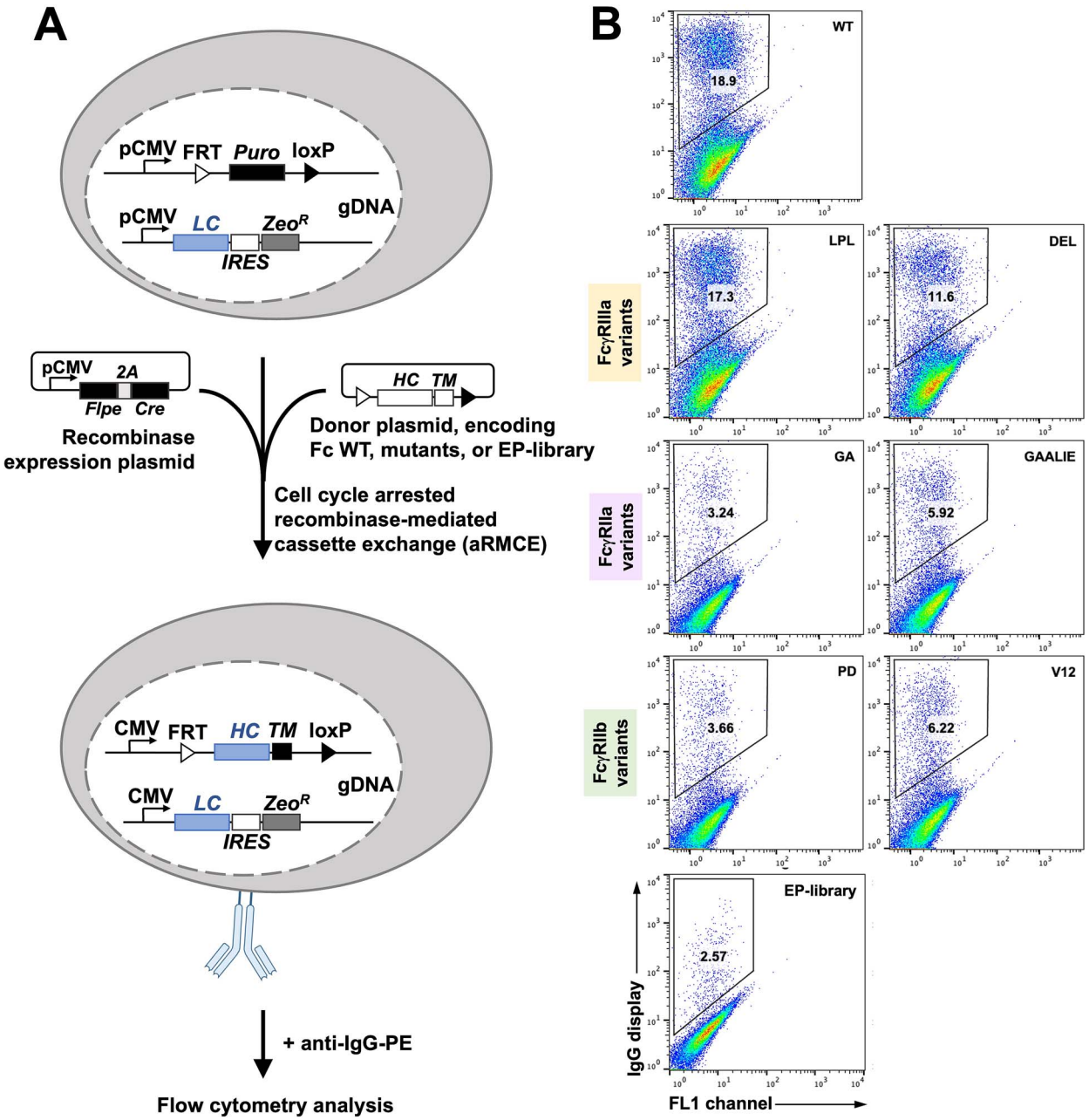

Figure 1. **High-efficiency genomic integration of Fc mutated antibody heavy chain genes via cell cycle arrested RMCE (aRMCE) and IgG display on CHO cell surface.** (**A**) Schematic. Following nocodazole treatment [34], monoclonal cells carrying a single RMCE landing pad and 3f8 light chain gene expression cassette on the genome were co-transfected with the recombinase expression plasmid and a promoter-less 3f8 heavy chain donor plasmid encoding Fc variants. The display of IgG was validated with anti-IgG-PE. (**B**) Flow cytometry analysis of transfected cells carrying Fc WT, known Fc mutants, and Fc error-prone library. Fc variants were grouped based on their associated FcγRs. 3f8 is an anti-TNFα mAb.

To deplete library cells lacking IgG display and to enrich Fc variants with high expression and/or high affinity, MACS was performed on streptavidin conjugated magnetic beads loaded with a mixture of biotinylated FcγRs [38] (Fig. 2A). The post-MACS library cells were then sorted for two sequential rounds with decreasing concentrations of FcγR targets using ratiometric gates which were determined with known Fc clones (Fig. 2C). More specifically, low affinity FcγRIIIa allotype 176F, a 1:1 mixture of FcγRIIa allotypes 131R and 131H, and FcγRIIb were used in separate FACS sorting processes. As results shown in Fig. 2C, rightward tilts gradually developed over the screening procedures, and after two rounds of FACS (post-R2) cell populations exhibited strong receptor bindings, suggesting successful isolations of affinity improved Fc clones towards each targeted FcγR.

Identification and validation of isolated Fc variants

To identify isolated Fc clones, genomic DNA was extracted from post-R2 populations, and the heavy chain genes encoding mutated Fc were recovered by PCR and subjected to subcloning and sequencing (Fig. 2A). For each FcγR target, 15-20 unique Fc variants were identified, and denoted as 3a, 2a, and 2b mutants, respectively. Sequence analysis revealed that isolated Fc variants carried 2.1 amino acid mutations on average (ranging from 1 to 6). Notably, 5 and 7 out of 15 identified 3a mutants

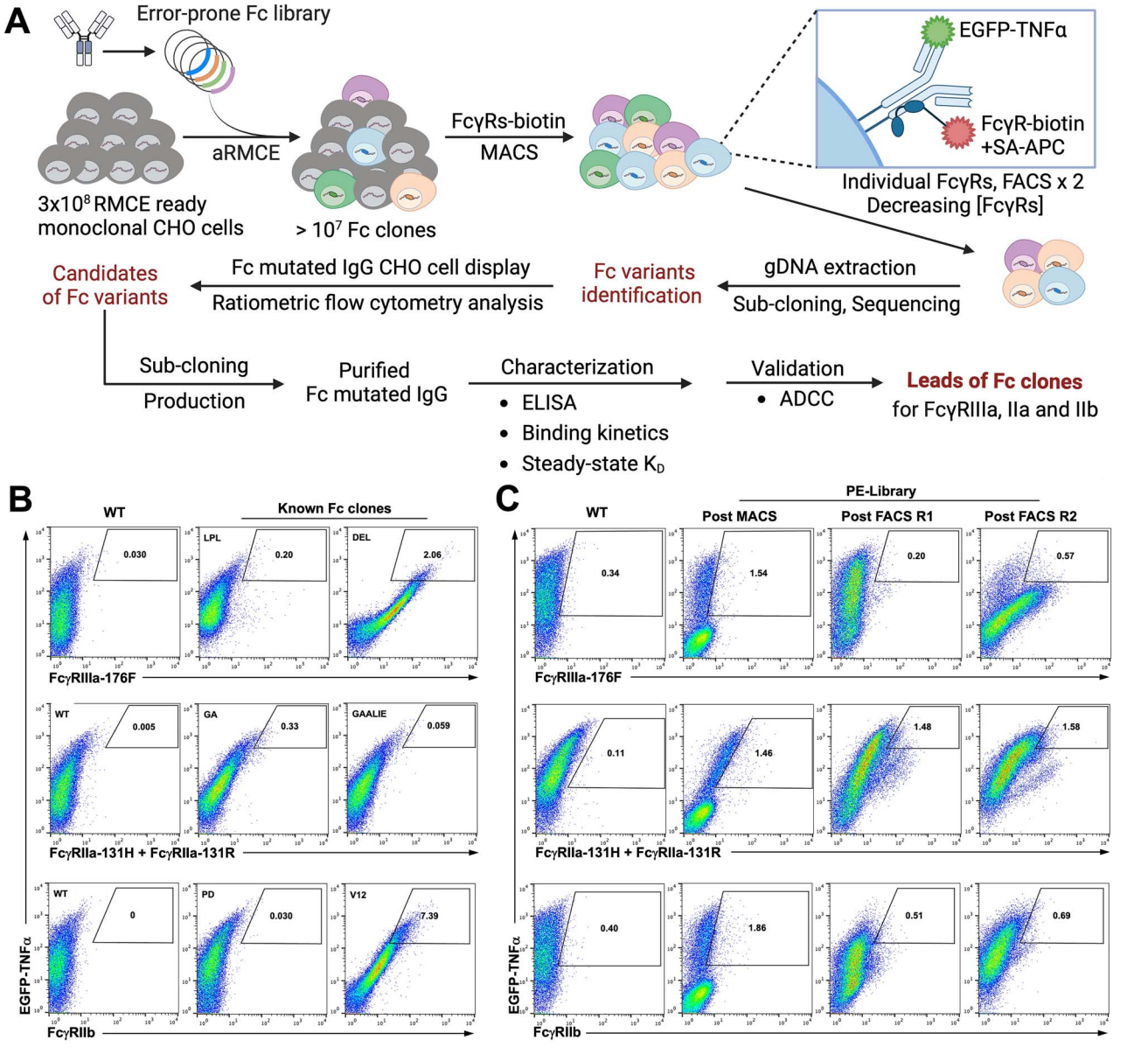

Figure 2. **Fc engineering by monoclonal mammalian cell display.** (**A**) Schematic of the process. Fc library plasmids carrying error-prone mutagenesis at the hinge-C_H2 region were introduced to RMCE ready CHO cells via aRMCE [34]. Transfected cells were incubated with FcγR bound beads for MACS to isolate IgG displaying cells. Post-MACS cells were screened by two rounds of FACS for the higher affinity towards FcγRIIIa-F176, FcγRIIa, and FcγRIIb, respectively. (**B**) Ratiometric flow cytometry analysis of Fc WT and known variants with antigen EGFR-TNFα, individual FcγR-biotin, and SA-APC. (**C**) Ratiometric flow cytometry analysis of library cells during the screening procedures.

(*i.e.*, towards FcγRIIIa-176F) had mutations at P247 and K334, respectively (Table 1). Such mutation hotspots were also found among 2a and 2b clones, including K290 for FcγRIIa binders, and K326 and L328 for FcγRIIb binders (Table S1, Table S2). To verify binding profiles of identified clones, Fc mutated IgGs were reconstituted on CHO-puro-3f8LC cell surface for further screening. Flow cytometry results showed that all identified 3a mutants achieved IgG display but at various degrees, ranging from 1.9 to 9.3% for IgG positive cells (Fig. 3, Fig. S1A). Furthermore, the majority of identified 3a mutants, except 3a-12, -13, and -15, demonstrated a clear rightward tilt towards FcγRIIIa-176F binding with significant increases on FcγRIIIa-176F^{high} cell postulations (gate R4 in Fig. S1A). Particularly, 1.15% of 3a-7 cells were FcγRIIIa-176F^{high}, 18- and 4.6-fold higher than the values for Fc WT and clone LPL (Fig. 3). It was also observed that some clones with tilted populations, *e.g.*, 3a-2 and 3a-9, showed moderate increases on FcγRIIIa-176F^{high} cell percentages, likely due to their low IgG display levels (Fig. S1A, Table 1). To address this issue, IgG positive cell populations were subjected to median fluorescence intensity (MFI) measurements on both FcγRIIIa-176F and antigen TNFα bindings, and then the MFI ratios were calculated to represent normalized FcγRIIIa-176F binding strength. Using this method, clone 3a-2 and 3a-9 had their MFI ratios at 11.1 and 9.2, representing 3.3- and 2.7-fold higher than that of Fc WT. Another important aspect of Fc variants is their binding selectivity, especially over the inhibitory FcγRIIb. Therefore, flow cytometry analyses were also conducted with FcγRIIb for normalized binding strength calculations (*i.e.*, MFI ratios between FcγRIIb and TNFα signals) (Fig. 3, Fig. S1B, Table 1). Results indicated that clones 3a-11 and 3a-14 had improved bindings on both FcγRIIIa and FcγRIIb, and thus were excluded from further consideration. Collectively, the selection criteria for 3a mutants include high

Table 1. Quantitative flow cytometry analysis of isolated FcγRIIIa-176F binders.

Clone	Mutations	Repeats	IgG$^+$ (%)	FcRIIIa-176F^{High} (%)	FcγRIIIa-176F MFI / TNFα MFI	FcγRIIb MFI / TNFα MFI
WT	-	-	13.9	0.064	3.4	2.6
LPL	F243L R292P Y300L	-	5.5	0.25	7.5	2.6
3a-1	P247L	1	2.7	0.10	8.0	5.2
3a-2	P247L K248E K334I	1	3.1	0.61	11.1	5.8
3a-3	P247H S254P	1	9.3	0.81	9.3	6.9
3a-4	P247L T256Y K290T	1	8.3	0.93	8.6	6.1
3a-5	P247H	1	6.9	0.80	9.6	7.1
3a-6	K334E	3	8.6	0.56	8.2	3.9
3a-7	K218I A231V K334E	5	8.7	1.15	8.9	6.1
3a-8	K334N	1	8.5	2.23	13.2	5.5
3a-9	F275I K288M K334I	1	1.9	0.21	9.2	5.0
3a-10	E293D K334E	1	7.4	0.14	6.9	3.5
3a-11	K274R K326E	1	8.4	0.83	9.8	12.9
3a-12	W277L	1	4.9	0.015	6.2	5.9
3a-13	V211D M252K H285R V305A L309Q K320M	1	8.8	0.025	3.9	4.0
3a-14	E269D K334E	1	3.0	1.15	16.6	10.8
3a-15	V282E	1	8.1	0.097	5.0	4.0

Notes: 1. MFIs (median fluorescence intensity) were calculated for IgG positive cell populations (Same for Table S1 & S2). 2. Selection criteria: high FcγRIIIa^{high} cell population (gate R4 in Fig. 3 & S1A), high FcγRIIIa over TNFα MFI ratio, low FcγRIIb over TNF MFI ratio, and good IgG display level (IgG$^+$ %). 3. Detrimental feature deselecting the clone shown in italic (Same for Table S1 & S2).

FcγRIIIa^{high} cell population, high FcγRIIIa over TNFα MFI ratio, low FcγRIIb over TNF MFI ratio, and ideally high IgG display level (Table 1). Applying these filters, 10 out of 15 identified 3a mutants passed. With similar selection criteria (Tables S1 & S2), parallel screenings were conducted for 2a and 2b mutants (Figs. S2 & S3). In conclusion, seven out of 18 identified 2a clones and six out of 20 identified 2b clones were excluded for a variety of reasons, including low FcγRIIa^{high} % or low normalized MFI ratio (2a-12, -14, -17, -18; 2b-16, -20), poor selectivity (2a-15; 2b-15, -17), and undesired mutations at C_H1 region (2a-13, -16; 2b-18, -19). All remaining clones were carried on for further biochemical characterizations.

Quantitation of improved affinity and selectivity

To measure binding affinities of selected Fc variants, trastuzumab carrying mutated Fc sequences were cloned and produced in 293F cells. The typical yields of Fc mutated IgGs were > 2 μg per ml of cell culture after purification. Produced IgGs were subjected to ELISA, in which biotinylated IgG was immobilized and signals were developed by anti-His-HRP targeting His tagged FcγRs. Results confirmed that except 3a-3 and -8, majority of selected 3a mutants showed enhanced binding strengths towards FcγRIIIa-176F, with their EC_{50} values ranging from 4.2 to 64.7 nM, indicating 5.8- to 89-fold improvements compared to that of WT Fc (Fig. 4A). We further tested binding selectivity of 3a mutants towards FcγRIIa and FcγRIIb (Fig. S4). To facilitate the analysis, all ELISA data were visualized as a heatmap, in which EC_{50} ratios of WT over Fc variants were calculated. As results summarized in Fig. 4B, clones 3a-2 and -7 improved their binding towards FcγRIIIa-176F by 56- and 89-fold, while their affinity increases on FcγRIIb were moderate. In contrast, clone 3a-4 had undesired lack of selectivity by showing improved bindings towards both FcγRIIIa-176F and FcγRIIb at similar degrees. Therefore, seven 3a clones were selected for further quantification by binding kinetics assays.

Using bio-layer interferometry, kinetic dissociation constants ($K_{D\text{-}K}$) were measured with both FcγRIIIa-176F and -176 V allotypes (Fig. S5A). Results indicated that all selected 3a mutants had reduced $K_{D\text{-}K}$ values compared to WT (Table 2), demonstrating the effectiveness of monoclonal IgG CHO cell display on Fc engineering. Specifically, variants 3a-1 (P247L) and 3a-5 (P247H), despite different mutations at the same site, showed comparable $K_{D\text{-}K}$ of 250 nM and 230 nM towards FcγRIIIa-176F. With two additional mutations, variant 3a-2 (P247L/K248E/K334I) exhibited a further reduction of K_D to 190 nM. Remarkably, variant 3a-7 (K218I/A231V/K334E) demonstrated the most significant 6-fold affinity enhancement towards FcγRIIIa-176F, surpassing the known clone LPL. Interesting, the affinity improvement trend was conserved towards the higher affinity allotype FcγRIIIa-176 V, suggesting the robustness of our screening approach. The selectivity of 3a clones was also measured with FcγRIIb, and the results suggested that most tested clones had binding enhancement on FcγRIIb but at less degrees compared to FcγRIIIa (Table 2). To further quantify the improved affinity, additional BLI experiments were conducted (Fig. S6) for determining steady-state apparent K_D ($K_{D\text{-}SS}$) values from Langmuir isotherm fitting (Fig. 5). Results indicated that 3a-2 and 3a-7 had $K_{D\text{-}SS}$ values of 370 nM and 250 nM towards FcγRIIIa-176F and 170 nM and 130 nM towards FcγRIIIa-176 V, overall representing a 2.6-fold improvement on average compared to WT Fc, similar to clone LPL (Table 3). Importantly, $K_{D\text{-}SS}$ of 3a-2 towards FcγRIIb was barely changed.

Parallel ELISA, kinetics and steady-state binding analyses were performed for 2a and 2b mutants as well. In ELISA, variants 2a-9, -10, and -11, all possessing a G236E mutation, exhibited increased affinity to FcγRIIa, reduced affinity to FcγRIIIa, and unchanged affinity to FcγRIIb (Fig. 4B, Fig. S4). Kinetic measurements confirmed binding improvements of these three 2a mutants towards FcγRIIa-131R, while 2a-10 showed the most significant enhancement ($K_{D\text{-}K}$ = 140 nM) (Fig. S5B, Table 2). Importantly, 2a-10 exhibited reduced binding strength to FcγRIIb (Fig. S5B, Table 2), suggesting a FcγRIIa specific variant. Moreover, steady-state binding analysis (Fig. S6, Fig. 5) confirmed that 2a-10 had an improved binding strength with $K_{D\text{-}SS}$ values of 250 and 290 nM towards FcγRIIa allotypes 131R and 131H, respectively (Table 3). Among 2b mutants, results collectively suggested that variant 2b-1 was a promising candidate with enhanced binding towards FcγRIIb (Figs. 4, 5, S4, S5C, S6; Tables 2, 3).

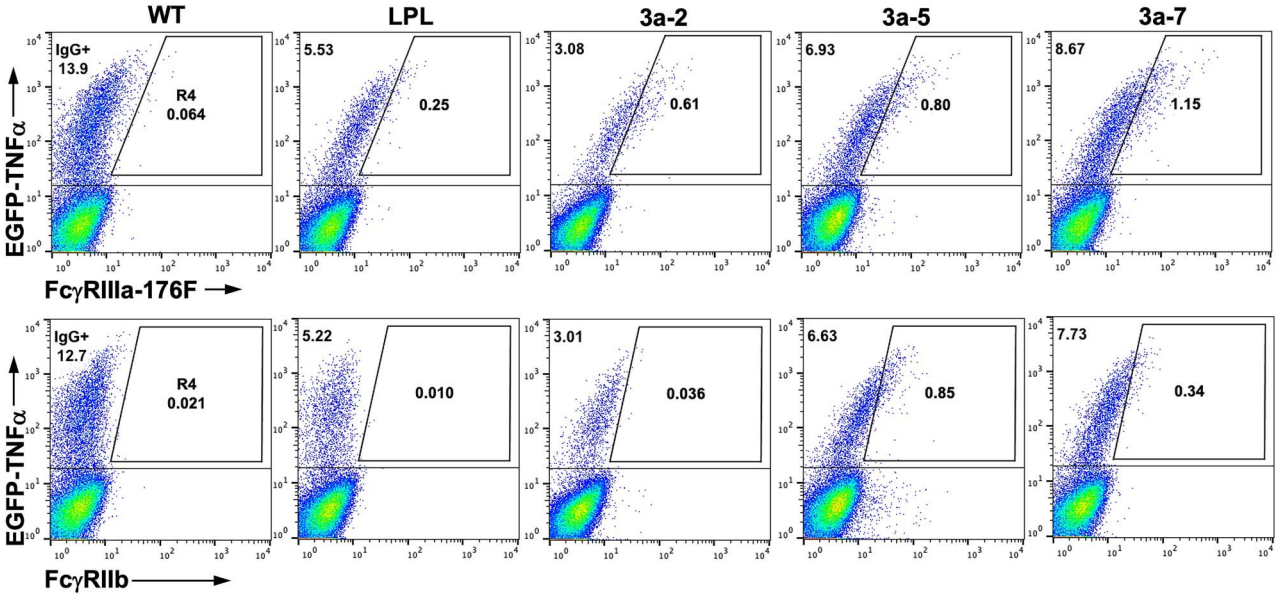

Figure 3. **Ratiometric flow cytometric analysis of isolated IIIa variants with FcγRIIIa-176F and FcγRIIb.** Cells were stained with EGFP-TNFα for IgG expression and biotinylated corresponding FcγRs and streptavidin-APC for FcγR binding. WT and LPL clones were used as controls. Table 1 shows quantitative analysis.

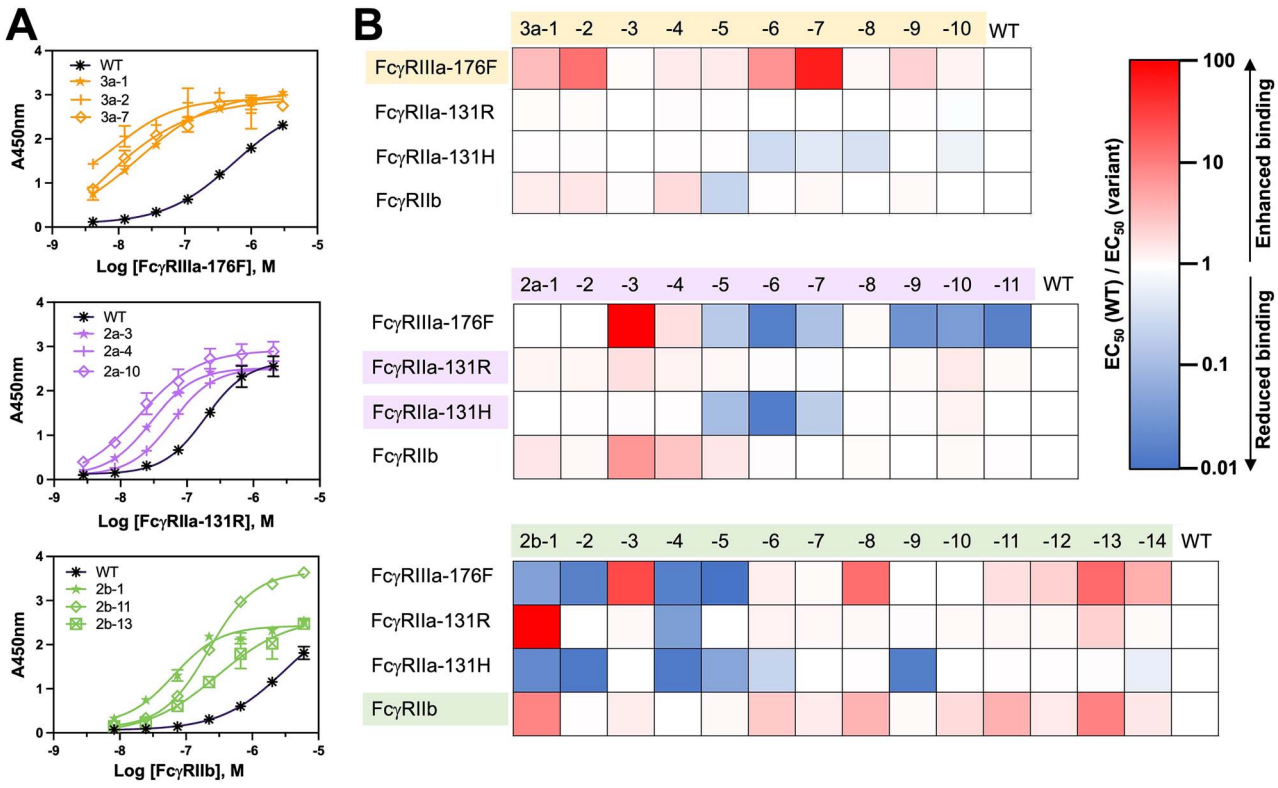

Figure 4. **ELISA of isolated Fc variants as trastuzumab IgG with FcγRs.** Bindings were measured on FcγRIIIa-176F, FcγRIIa-131R, FcγRIIa-131H, and FcγRIIb, respectively (n = 3). (**A**) Sigmoidal curving fitting of WT and representative Fc variants. (**B**) Heat maps indicating binding enhancement or reduction, which were measured by ratios of ELISA EC_{50} of WT over Fc variants, calculated by the equation EC_{50} WT/EC_{50} variant.

Isolated 3a variants showed enhanced ADCC activity

To assess effector functions mediated by the isolated Fc variants, cellular ADCC assays were conducted, in which MDA-MB-231-BR-HER2 breast cancer cells and human PBMC were used as the target and effector cells, respectively. In the presence of trastuzumab bearing WT Fc or 3a mutants, cell lyses were monitored in real-time, and sigmoidal curves were generated responding to IgG concentrations. After 56 hours of antibody addition, significant cytotoxicity was observed for variant 3a-2, 3a-5, and 3a-7 with their potencies of 2.0, 3.7, and 4.9 ng/mL, representing 3-7 folds improvement over WT Fc (EC_{50} = 13.3 ng/mL, Fig. 6).

Table 2. Kinetic binding affinity ($K_{D\text{-}K}$, nM).

Clone	FcγRIIIa-176F	FcγRIIIa-176 V	FcγRIIa-131R	FcγRIIa-131H	FcγRIIb
WT	640 ± 76	430 ± 50	330 ± 83	240	570 ± 64
3a-1	250	250	n.d.		430
3a-2	190	100			160
3a-5	230	200			210
3a-7	110	100			280
3a-8	320	220			310
3a-9	440	220			280
3a-10	340	250			340
LPL	290	110			320
2a-9	n.d.		210	400	600
2a-10			140	220	1100
2a-11			220	490	2600
GA			130	150	440
2b-1	800	n.d.	160	n.d.	180
2b-5	2500		240		430
2b-7	530		190		210
2b-10	530		170		280
PD	> 5000		1250		450

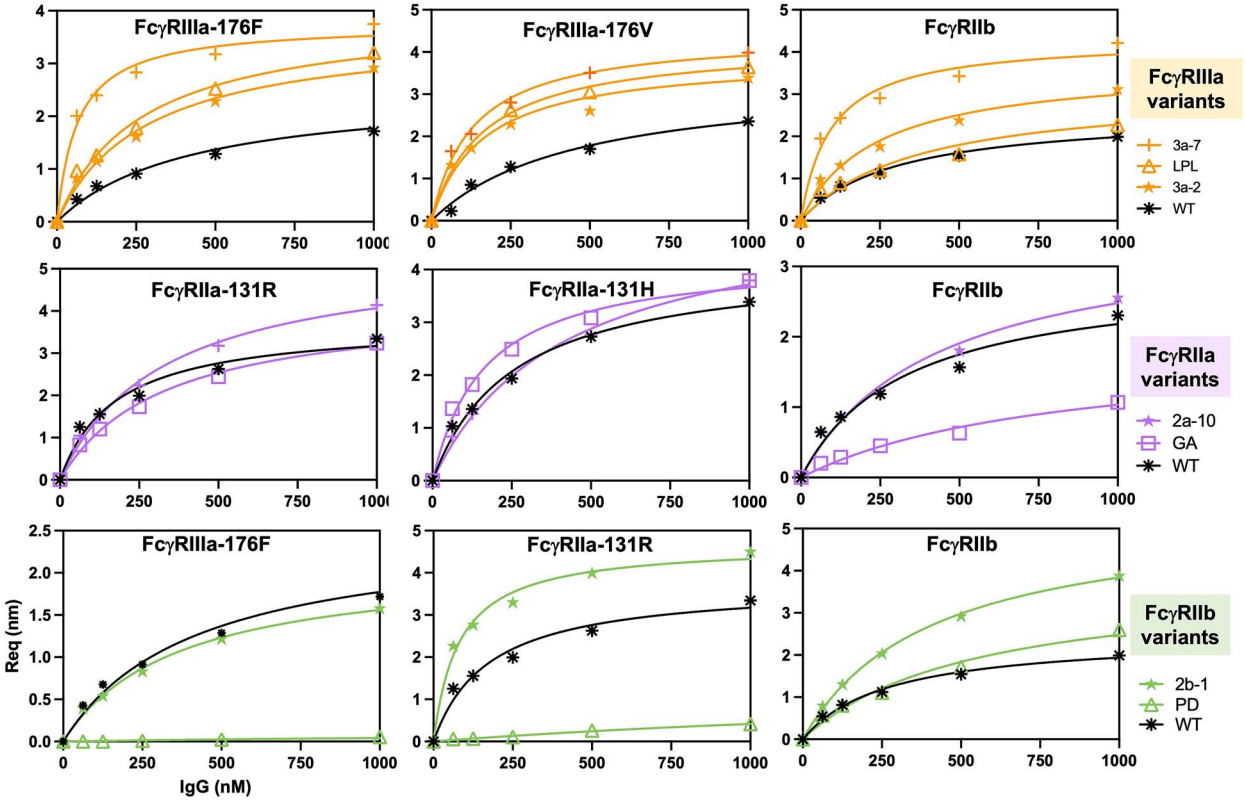

Figure 5. **Equilibrium responses.** Biotinylated FcγRs loaded streptavidin biosensors were subjected to the association with purified IgGs at five decreasing concentrations, and the dissociation with PBS. Steady-state dissociation constants ($K_{D\text{-}SS}$) were calculated from a Langmuir isotherm, and shown in Table 3.

Discussion

The construction of combinatorial libraries in a monoclonal manner and the expression of the diversified protein targets in their functional form are two desired prerequisites for any directed evolution endeavor. In regard to Fc engineering, microbial systems such as *E. coli* periplasmic and yeast surface displays cannot produce the mammalian glycosylation needed for recognitions of FcγRs and complement factors. And the popular methods of library construction in mammalian cells, *e.g.*, by utilizing episomal plasmids or lentiviruses, also have noted drawbacks such as transgene instability, polyclonality, and transcriptional variation. This study leveraged a newly developed approach termed aRMCE [34] that enables precise integration of mutated Fc genes to a single landing pad in a defined genomic context, and thus achieved monoclonality (one Fc variant per cell) and transcriptional normalization. Furthermore, the high integration efficiency of aRMCE

Table 3. Steady-state binding affinity ($K_{D\text{-}SS}$, nM).

Clone	FcγRIIIa-176F	FcγRIIIa-176 V	FcγRIIa-131R	FcγRIIa-131H	FcγRIIb
WT	770	390	520	390	580
3a-2	370	170	n.d.		560
3a-7	250	130			290
LPL	270	160			700
2a-10	n.d.		250	290	980
GA			260	170	1300
2b-1	600	n.d.	80	n.d.	240
PD	n.b.		5400		650

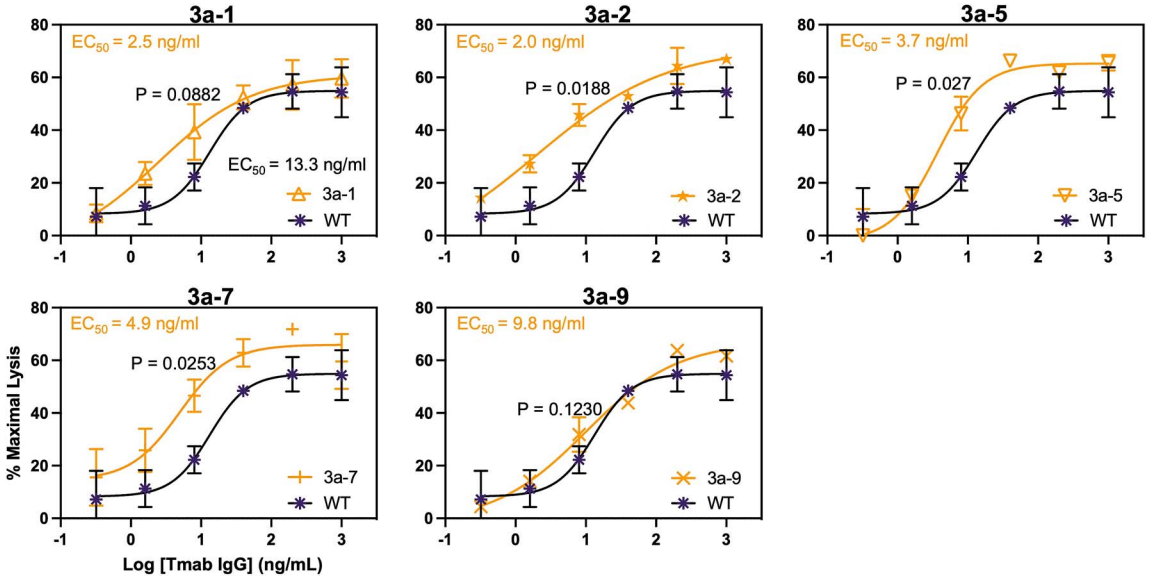

Figure 6. **ADCC of Fc mutated trastuzumab.** PBMC was used as effector cells and HER2-positive MDA-MB-231 as target cells (E:T = 15:1, n = 2).

streamlined the process: a single transfection of 3×10^8 CHO cells yielded an Fc mutagenesis library of 7.5×10^6 functional clones, circumventing the tedious and time-consuming virus packaging procedures. Due to the nature of error-prone PCR, stop codons and silent mutations were introduced inevitably, therefore with more efficient mutagenesis design, larger functional diversities should be achievable. Another important aspect of our approach was the full-length IgG display, which allowed ratiometric FACS on FcγRs and antigen, practically mimicking the effector cell recruitment event, and more effective than the tag-based monitoring of Fc display level previously used. Interestingly, we found that certain mutations at the lower C_H1 and hinge region (*e.g.*, D221G, H224R) caused reduced binding to the antigen TNFα while maintaining their affinities towards FcγRs (data not shown), underscoring the importance of displaying full-length IgG in the selection of functional Fc variants.

By combining monoclonal integration at defined genome locus, full-length IgG display, and ratiometric flow cytometry, our method accurately distinguished known Fc clones from WT (Fig. 2B). And by one round of MACS and two rounds of FACS, panels of Fc variants of improved affinity and selectivity were isolated, without mutation combination or shuffling often conducted in previous studies [22, 25]. To validate and characterize affinity-improved Fc variants, clone reconstitution and IgG production were carried out and multiple quantitative approaches were applied including flow cytometry, ELISA, kinetic and steady-state binding affinity measurements. We believe employing multifaceted evaluation approaches can reduce the bias given by certain experimental system or assay. Collectively, clones such as 3a-1, 3a-2, 2a-10, 2a-11, and 2b-1 showed significant and specific binding improvements towards their corresponding receptors. Particularly, 3a-2 exhibited $K_{D\text{-}K}$ of 190 nM and 100 nM towards FcγRIIIa allotypes, and 2.0 ng/ml potency in ADCC assays, which were dramatic enhancements compared to WT Fc. Worth mentioning, several Fc variants (such as 3a-2 and 3a-7) showed enhanced cytotoxic efficacy with both tested target cell lines SKOV3 [34] and MDA-MB-231-BR-HER2 (Fig. 6), suggesting robustness of the isolated clones. Mutation site analysis of isolated variants revealed that in addition to the interface residues (*e.g.*, 232, 236, 266, 267, 326, 328, 334) suggested by structural studies [23, 39–41] and previous Fc engineering works [22, 25, 33, 42, 43], random mutagenesis and selection in CHO cells discovered new mutation sites including P247H/L for FcγRIIIa, K290E for FcγRIIa, and K334E/I for FcγRIIb (Fig. 7). These hotspots are worth for future investigation such as by site-saturation mutagenesis or focused library designs.

This study can be improved through: (1) incorporating negative screening to improve binding selectivity; (2) combining kinetic and equilibrium selection to isolate Fc variants with slow off rates, a beneficial feature for efficient immune cell recruitments; (3) incorporating defucosylation designs to further enhance FcγR recognition; and (4) testing isolated 2a mutants on ADCP, and 2b mutants in agonist antibody activation assays. Moving forward, we envision that construction of high-quality large-diversity

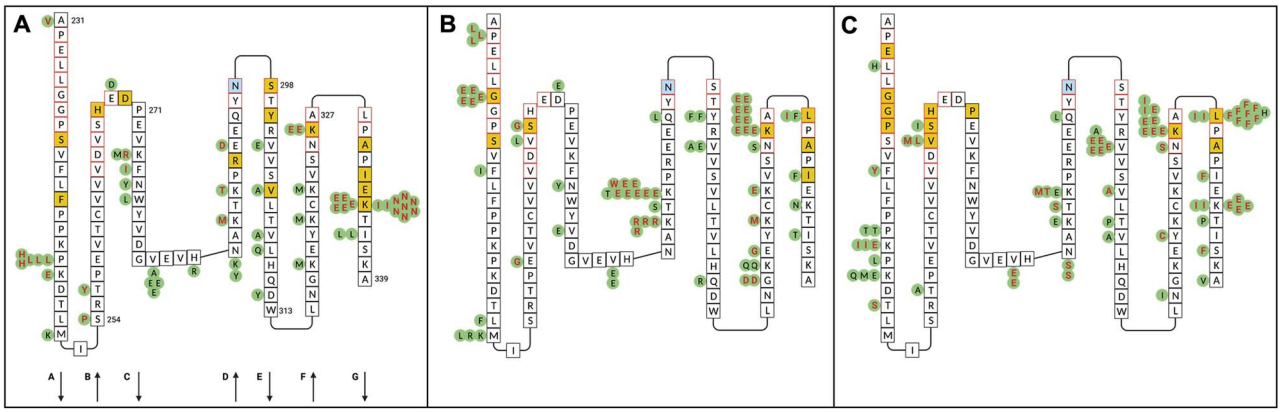

Figure 7. **Two-dimensional collier de Pearles representations of the IgG1 CH2 domain showing identified mutations towards (A) FcγRIIIa-F176, (B) FcγRIIa (both -H131 and -R131 allotypes), and (C) FcγRIIb.** Green circles represent all mutations identified in this study, among which the ones with improved affinity confirmed by ELISA are shown with red letters; yellow shades represent the beneficial mutation sites reported in literatures; red boxes represent the residues interact with FcγRs; blue shades represent the glycosylation site. Antiparallel β strands within the CH2 domain fold are also shown.

Fc mutagenesis libraries in mammalian cells should enable Fc engineering to (1) precisely delineate the functions of individual FcγRs, a crucial step for customizing therapeutic mAbs to optimize patient outcomes; (2) achieve complete effector function silencing, a key attribute for applications such as receptor blocking antibodies; and (3) manipulate interactions between antibody isotypes other than IgG, *e.g.*, IgA/IgM/IgE, and their associated receptors. Notably, all these prospective tasks of Fc engineering cannot be readily accomplished by current technologies of either rational designs or microbial display. In summary, by overcoming methodological limitations via aRMCE mammalian cell IgG display, Fc variants with improved affinity and selectivity towards FcγRs were isolated and novel mutation hotspots were discovered. These findings are valuable for designing next-generation Fc libraries, incorporating machine learning into Fc optimization, and advancing therapeutic antibody development.

Methods

Plasmid construction

C_H2 fragments encoding Fc mutants, including LPL(F243L/R293P/Y300L) [25], DEL (S239D/I332E/A330L) [21], GA (G236A) [17], GAALIE (G236A/I332E/A330L) [17], PD (P238D) [22], V12 (E233D/G237D/P238D/H268D/P271G/A330R) [22], were generated by site-directed mutagenesis using overlapping primers, then cloned to pEx-3f8HC [34] with BstXI and BsrGI to give associated heavy chain exchange plasmids. Genes encoding trastuzumab heavy chain and light chain were chemically synthesized (IDT). The light chain was cloned to pCIW-BirA-IRES-Hy [38] with XhoI and HpaI, giving pCIW-TrastLC-IRES-Hy. The heavy chain was fused with chimeric intron at the N-terminus with overlapping PCR and cloned into pCIW-3f8LC-IRES-Zeo [34] with NheI and PmlI, yielding pCIW-TrastHC-IRES-Zeo. For C-terminal biotinylation, the heavy chain was fused with a $(GGGGS)_2$ linker and AviTag with overlapping PCR and cloned to pCIW-TrastHC-IRES-Zeo via BsrGI and KpnI, giving pCIW-TrastHC-Avitag-IRES-Zeo. The Fc variants were sub-cloned from pEx-3f8HC to the WT trastuzumab HC or HC-Avitag expression plasmids via BstXI and BsrGI.

Cell lines and cell culture

CHO-Puro-3f8LC cells [34] and human cancer cell line MDA-MB-231-BR-HER2 (gifted from Dr. Patricia Steeg at NCI) were maintained in Ham's F-12 K (Kaighn's) medium (Corning, Cat#10–025) and DMEM medium (Corning, Cat#10–013), respectively, supplemented with 10% fetal bovine serum (FBS, Gibco, Cat# 10437028), 50 U/ml penicillin, and 50 μg/ml streptomycin (Gibco, Cat#15140122) at 37 °C, in 5% CO_2 humidified atmosphere. Expi293F (Gibco, Cat#A14527) was cultured in Expi293 medium (Gibco, Cat#A1435101) supplemented with 40 U/ml penicillin and 40 μg/ml streptomycin at 37 °C, in 8% CO_2 humidified atmosphere with a shaking speed of 130 rpm.

Transfection for cell cycle aRMCE

CHO-Puro-3f8LC cells were seeded at 3.5×10^5 cells per well in 6-well plates and cultured for 24 h to achieve over 80% confluency. Culture supernatants were replaced with 1.8 mL fresh F-12 K media containing 650 nM nocodazole. After 30-min incubation, 0.2 mL transfection mixtures containing 1 μg exchange plasmid, 1 μg pF2AC [34], and 8 μg PEI were added to cells. After 20-h cultivation, cells were detached and cultured in a new plate with fresh media.

Cell isolation by magnetic-activated cell sorting

Library cells were harvested, washed twice with 0.5% BSA in PBS (PBSA) and subjected to MACS. More specifically, cells were incubated at 4 °C for 30 min with a mixture of biotinylated FcγRs containing 100 nM FcγRIIIa-F176, 50 nM FcγRIIIa-V176, 50 nM FcγRIIa-H131, 50 nM FcγRIIa-R131 and 200 nM FcγRIIb, then washed twice with PBSA and incubated with streptavidin MicroBeads (Miltenyi Biotec) at 4 °C for 15 min with occasional inversion. After washing and resuspending in 3 mL PBSA, the samples were loaded to a pre-rinsed LS magnetic column attached to a QuadroMACS separator (Miltenyi Biotec) and washed three times with 3 mL PBSA. The column was then removed from the magnet and cells were collected by flushing with 5 mL PBSA. Eluted cells were further cultured for expansion.

Flow cytometry and FACS

Cells displaying human mAb were stained with 1 μg/ml mouse anti-human IgG (Fab)-PE (Invitrogen Cat#MA1–10377). Cells were recovered at 37 °C for 30 min and added with 4 mL fresh media for cultivation. Flow cytometry analysis and sorting were performed on S3e (Bio-Rad) or Aria II (BD). Post-MACS cells were cultured

and resuspended in 2 mL PBSA and incubated with 60 nM EGFP-TNFα and biotinylated FcγRs at 4 °C for 30 min. More specifically, 80 nM FcγRIIIa-F176, 90 nM FcγRIIa-H131 plus 110 nM FcγRIIa-131R, and 160 nM FcγRIIb were used in the first round of FACS, and 50 nM FcγRIIIa-176F, 60 nM FcγRIIa-131H plus 70 nM FcγRIIa-131R, and 130 nM FcγRIIb were used in the second round of FACS. Cells were then washed twice with PBSA, incubated with 1 μg/ml streptavidin-APC (Invitrogen Cat# 17–4317-82) in PBSA at 4 °C for 15 min. After washing twice with PBSA, cells having high APC to EGFP signal ratio were sorted on S3e cell sorter (Bio-Rad) with a typical gate of ∼1% cells at a speed of 2 000–3 000 events per s. Enrich mode was used for the first round and purity mode for the second round. For monoclonal flow cytometry analysis, CHO-Puro-3f8LC cells transfected with pEx-HC carrying the isolated Fc mutants were stained with 60 nM EGFP-TNFα, biotinylated FcγRs (40 nM FcγRIIIa-176F, 45 nM FcγRIIa-131H plus 55 nM FcγRIIa-131R, or 80 nM FcγRIIb) and 1 μg/ml SA-APC.

Fc mutants identification

The genomic DNA of isolated cells was extracted using Wizard Genomic DNA Purification Kit (Promega, Cat#A1120), and the heavy chain genes were amplified by PCR with 1 μg gDNA as the template by using Q5-High Fidelity DNA polymerase (NEB). The thermal cycling program was 98 °C for 30 s; 30 cycles of 98 °C for 10 s, 63 °C for 20 s, 72 °C for 40 s; final extension at 72 °C for 2 min and storage at 4 °C. The PCR products were gel purified, digested with BstXI and BsrGI, and cloned into the exchange plasmid pEx-HC. Colonies were randomly picked for minipreps and sequencing to identify isolated Fc mutants.

Recombinant protein production and purification

EGFP-TNFα was produced using *E. coli* BL21(DE3) in Luria Bertani media with 1 mM IPTG induction at room temperature for 12 h, and purified from sonicated cell lysis using HisPur Ni-NTA resin. The extracellular domains of human FcγRs FcγRIIIa-176F, FcγRIIIa-176 V, FcγRIIa-131H, FcγRIIa-131R, and FcγRIIb, including their biotinylated proteins were produced as described previously [38]. Trastuzumab IgGs carrying WT and mutated Fc were produced in a 30 mL cell culture by transient transfecting pCIW-TrastHC-IRES-Zeo to Expi293F cell line stably expressing trastuzumab light chain [44]. Biotinylated IgGs were produced by fusing AviTag to C termini of the heavy chain genes, and co-expression with endoplasmic reticulum (ER)-retained BirA in a 4 mL cell culture. All IgGs were purified by protein A resin (GenScript) five days post transfection.

ELISA

Maxisorp 96-well plates (Thermo Scientific, Cat#439454) were coated with 100 μL of 5 μg/ml streptavidin (NEB) at 4 °C overnight and then blocked with 2% BSA in PBS (2% PBSA) at room temperature (RT) for 2 h. 100 μL of 2 μg/ml biotinylated IgGs were added for incubation at RT for 45 min, and plates were washed four times with PBS supplemented with 0.05% Tween-20 (PBST) and twice with PBS. FcγRIIIa-176F, FcγRIIa-131H and FcγRIIa-131R starting at 3 μM and FcγRIIb starting at 6 μM were 1:3 serially diluted with 2% PBSA and added by 100 μL to each well. After 1 h incubation at RT and washing as described above, 100 μL anti-His-HRP at 1:10,000 dilution (Abcam, Cat#ab1187) was added. Plates were incubated at RT for 1 h and washed. 50 μL TMB (Thermo Scientific, Cat# 34028) was added each well to develop the signals. The reaction was terminated by adding 50 μL 2 M H_2SO_4, and the absorbance at 450 nm was measured with an Epoch microplate reader (BioTek). ELISA experiments were performed in duplicates.

Binding kinetics measurements

Binding kinetics were measured in PBS at 25 °C by bio-layer interferometry (BLI) using BLItz (FortéBio). 5 μg/ml of biotinylated FcγRs were loaded on streptavidin biosensors (FortéBio, Cat# 18–5019) for 2 min. The association was monitored for 1 min with purified IgGs at five decreasing concentrations, and the dissociation was monitored with PBS for 2 min. Kinetic analyses were performed with BLItz Pro software using its 1:1 fitting model. Steady-state dissociation constants ($K_{D\text{-}SS}$) were calculated from a Langmuir isotherm: $R_{eq} = R_{max} * C/(K_D + C)$ where R_{eq} is the equilibrium response at each antibody concentration C, and R_{max} is the maximum specific binding response obtained from fitting. The sensorgrams were obtained with GraphPad Prism 9.

Antibody-dependent cellular cytotoxicity

ADCC was measured by a non-invasive gold microelectrode-based cell cytotoxicity assay with xCELLigence instrument (ACEA Biosciences). 1×10^4 MDA-MB-231-BR-HER2 cells were seeded to E-Plate 96. After 4 h cultivation, 1.5×10^5 peripheral blood mononuclear cells (PBMC) purified from healthy human blood were added as effector cells. Antibodies were added in 5-fold dilutions starting from 1 μg/ml, and the cell index (I) was monitored continuously for 4 days. Samples without adding antibodies were used as controls. The cell indices recorded after 56 h of treatment were used to calculate the percentage of cell lysis using the formula:

$$\frac{I_{control} - I_{treatment}}{I_{control}} \times 100\%$$

Each measurement was performed as duplicates and the standard deviation is shown in the plots.

Ethics and consent statement

Not applicable.

Animal research

No animal studies were involved.

Author contributions

Zening Wang: Conceptualization (Equal), Data curation (Lead), Formal Analysis (Equal), Investigation (Lead), Methodology (Lead), Visualization (Lead), Writing—original draft (Lead), Writing—review & editing (Equal); Minhyo Kang: Data curation (Supporting), Investigation (Supporting), Writing—review & editing (Supporting); Afshin Ebrahimpour: Data curation (Supporting); Chuan Chen: Conceptualization (Supporting), Investigation (Supporting); Xin Ge: Conceptualization (Lead), Formal Analysis (Equal), Funding acquisition (Lead), Supervision (Lead), Visualization (Equal), Writing—original draft (Equal), Writing—review & editing (Lead).

Supplementary Data

Supplementary data are available at ABT Online.

Conflict of interest

None declared.

Funding

This work is supported by National Institute of General Medical Sciences grants R01GM115672 and R35GM141089 to X.G.

Data availability

The data underlying this article are available in the article and in its online supplementary material.

References

1. Casadevall, A, Dadachova, E, Pirofski, L. Passive antibody therapy for infectious diseases. *Nat Rev Microbiol* 2004; **2**: 695–703. https://doi.org/10.1038/nrmicro974.
2. Scott, AM, Wolchok, JD, Old, LJ. Antibody therapy of cancer. *Nat Rev Cancer* 2012; **12**: 278–87. https://doi.org/10.1038/nrc3236.
3. Chan, AC, Carter, PJ. Therapeutic antibodies for autoimmunity and inflammation. *Nat Rev Immunol* 2010; **10**: 301–16. https://doi.org/10.1038/nri2761.
4. Yasunaga, M. Antibody therapeutics and Immunoregulation in cancer and autoimmune disease. *Semin Cancer Biol* 2020; **64**: 1–12. https://doi.org/10.1016/j.semcancer.2019.06.001.
5. Nimmerjahn, F, Ravetch, JV. Fcγ receptors as regulators of immune responses. *Nat Rev Immunol* 2008; **8**: 34–47. https://doi.org/10.1038/nri2206.
6. Hogarth, PM, Pietersz, GA. Fc receptor-targeted therapies for the treatment of inflammation, cancer and beyond. *Nat Rev Drug Discov* 2012; **11**: 311–31. https://doi.org/10.1038/nrd2909.
7. Bournazos, S, Corti, D, Virgin, HW. *et al.* Fc-optimized antibodies elicit CD8 immunity to viral respiratory infection. *Nature* 2020; **588**: 485–90. https://doi.org/10.1038/s41586-020-2838-z.
8. Liu, R, Oldham, RJ, Teal, E. *et al.* Fc-engineering for modulated effector functions—improving antibodies for cancer treatment. *Antibodies* 2020; **9**: 64. https://doi.org/10.3390/antib9040064.
9. Horst, HJ v D, Nijhof, IS, Mutis, T. *et al.* Fc-engineered antibodies with enhanced fc-effector function for the treatment of B-cell malignancies. *Cancer* 2020; **12**: 3041. https://doi.org/10.3390/cancers12103041.
10. Yamin, R, Jones, AT, Hoffmann, H-H. *et al.* Fc-engineered antibody therapeutics with improved anti-SARS-CoV-2 efficacy. *Nature* 2021; **599**: 465–70. https://doi.org/10.1038/s41586-021-04017-w.
11. Treon, SP, Hansen, M, Branagan, A. *et al.* Polymorphisms in FcγRIIIA (CD16) receptor expression are associated with clinical response to rituximab in Waldenstrom's macroglobulinemia. *J Clin Oncol Official J Am Soc Clin Oncol* 2004; **22**: 6556. https://doi.org/10.1200/jco.2004.22.90140.6556.
12. Cartron, G, Dacheux, L, Salles, G. *et al.* Therapeutic activity of humanized anti-CD20 monoclonal antibody and polymorphism in IgG fc receptor FcγRIIIa gene. *Blood* 2002; **99**: 754–8. https://doi.org/10.1182/blood.V99.3.754.
13. Gavin, PG, Song, N, Kim, SR. *et al.* Association of Polymorphisms in FCGR2A and FCGR3A with degree of Trastuzumab benefit in the adjuvant treatment of ERBB2/HER2–positive breast cancer: analysis of the NSABP B-31 trial. *JAMA Oncol* 2016; **3**: 335–41. https://doi.org/10.1001/jamaoncol.2016.4884.
14. Bibeau, F, Lopez-Crapez, E, Fiore, FD. *et al.* Impact of FcγRIIa-FcγRIIIa polymorphisms and KRAS mutations on the clinical outcome of patients with metastatic colorectal cancer treated with Cetuximab plus Irinotecan. *J Clin Oncol* 2009; **27**: 1122–9. https://doi.org/10.1200/JCO.2008.18.0463.
15. Yee, AMF, Phan, HM, Zuniga, R. *et al.* Association between FcγRIIa-R131 Allotype and Bacteremic pneumococcal pneumonia. *Clin Infect Dis* 2000; **30**: 25–8. https://doi.org/10.1086/313588.
16. Sorge, NMV, Pol, WVD, Winkel, JGJVD. FcγR polymorphisms: implications for function, disease susceptibility and immunotherapy. *Tissue Antigens* 2003; **61**: 189–202. https://doi.org/10.1034/j.1399-0039.2003.00037.x.
17. Richards, JO, Karki, S, Lazar, GA. *et al.* Optimization of antibody binding to FcγRIIa enhances macrophage phagocytosis of tumor cells. *Mol Cancer Ther* 2008; **7**: 2517–27. https://doi.org/10.1158/1535-7163.MCT-08-0201.
18. Mayes, PA, Hance, KW, Hoos, A. The promise and challenges of immune agonist antibody development in cancer. *Nat Rev Drug Discov* 2018; **17**: 509–27. https://doi.org/10.1038/nrd.2018.75.
19. Li, F, Ravetch, JV. Inhibitory Fcγ receptor engagement drives adjuvant and anti-tumor activities of agonistic CD40 antibodies. *Science* 2011; **333**: 1030–4. https://doi.org/10.1126/science.1206954.
20. Garris, CS, Wong, JL, Ravetch, JV. *et al.* Dendritic cell targeting with fc-enhanced CD40 antibody agonists induces durable antitumor immunity in humanized mouse models of bladder cancer. *Sci Transl Med* 2021; **13**: 13. https://doi.org/10.1126/scitranslmed.abd1346.
21. Lazar, GA, Dang, W, Karki, S. *et al.* Engineered antibody fc variants with enhanced effector function. *Proc National Acad Sci* 2006; **103**: 4005–10. https://doi.org/10.1073/pnas.0508123103.
22. Mimoto, F, Katada, H, Kadono, S. *et al.* Engineered antibody fc variant with selectively enhanced FcγRIIb binding over both FcγRIIaR131 and FcγRIIaH131. *Protein Engineering, Design and Selection* 2013; **26**: 589–98. https://doi.org/10.1093/protein/gzt022.
23. Wang, X, Mathieu, M, Brezski, RJ. IgG fc engineering to modulate antibody effector functions. *Protein Cell* 2018; **9**: 63–73. https://doi.org/10.1007/s13238-017-0473-8.
24. Delidakis, G, Kim, JE, George, K. *et al.* Improving antibody therapeutics by manipulating the fc domain: immunological and structural considerations. *Annu Rev Biomed Eng* 2022; **24**: 249–74. https://doi.org/10.1146/annurev-bioeng-082721-024500.
25. Stavenhagen, JB, Gorlatov, S, Tuaillon, N. *et al.* Fc optimization of therapeutic antibodies enhances their ability to kill tumor cells In vitro and controls tumor expansion In vivo via low-affinity activating Fcγ receptors. *Cancer Res* 2007; **67**: 8882–90. https://doi.org/10.1158/0008-5472.CAN-07-0696.
26. Jung, ST, Reddy, ST, Kang, TH. *et al.* Aglycosylated IgG variants expressed in bacteria that selectively bind FcγRI potentiate tumor cell killing by monocyte-dendritic cells. *Proc National Acad Sci* 2010; **107**: 604–9. https://doi.org/10.1073/pnas.0908590107.
27. Jung, ST, Kelton, W, Kang, TH. *et al.* Effective phagocytosis of low Her2 tumor cell lines with engineered, Aglycosylated IgG displaying high FcγRIIa affinity and selectivity. *ACS Chem Biol* 2013; **8**: 368–75. https://doi.org/10.1021/cb300455f.
28. Kang, TH, Lee, C-H, Delidakis, G. *et al.* An engineered human fc variant with exquisite selectivity for FcγRIIIaV158 reveals that ligation of FcγRIIIa mediates potent antibody dependent cellular phagocytosis with GM-CSF-differentiated macrophages. *Front Immunol* 2019; **10**: 562. https://doi.org/10.3389/fimmu.2019.00562.
29. Lee, C-H, Romain, G, Yan, W. *et al.* IgG fc domains that bind C1q but not effector Fcγ receptors delineate the importance of complement-mediated effector functions. *Nat Immunol* 2017; **18**: 889–98. https://doi.org/10.1038/ni.3770.
30. Jennewein, MF, Alter, G. The Immunoregulatory roles of antibody glycosylation. *Trends Immunol* 2017; **38**: 358–72. https://doi.org/10.1016/j.it.2017.02.004.

31. Jefferis, R. Recombinant antibody therapeutics: the impact of glycosylation on mechanisms of action. *Trends Pharmacol Sci* 2009; **30**: 356–62. https://doi.org/10.1016/j.tips.2009.04.007.
32. Liu, Y, Lee, AG, Nguyen, AW. *et al.* An antibody fc engineered for conditional antibody-dependent cellular cytotoxicity at the low tumor microenvironment pH. *J Biol Chem* 2022; **298**: 101798. https://doi.org/10.1016/j.jbc.2022.101798.
33. Chen, D, Zhao, Y, Li, M. *et al.* A general fc engineering platform for the next generation of antibody therapeutics. *Theranostics* 2021; **11**: 1901–17. https://doi.org/10.7150/thno.51299.
34. Chen, C, Wang, Z, Kang, M. *et al.* High-fidelity large-diversity monoclonal mammalian cell libraries by cell cycle arrested recombinase-mediated cassette exchange. *Nucleic Acids Res* 2023; **51**: e113–3. https://doi.org/10.1093/nar/gkad1001.
35. Turan, S, Zehe, C, Kuehle, J. *et al.* Recombinase-mediated cassette exchange (RMCE) — a rapidly-expanding toolbox for targeted genomic modifications. *Gene* 2013; **515**: 1–27. https://doi.org/10.1016/j.gene.2012.11.016.
36. Grindley, NDF, Whiteson, KL, Rice, PA. Mechanisms of site-specific recombination*. *Annu Rev Biochem* 2006; **75**: 567–605. https://doi.org/10.1146/annurev.biochem.73.011303.073908.
37. Brezski, RJ, Georgiou, G. Immunoglobulin isotype knowledge and application to fc engineering. *Curr Opin Immunol* 2016; **40**: 62–9. https://doi.org/10.1016/j.coi.2016.03.002.
38. Kang, M, Wang, Z, Ge, X. One-step production of fully biotinylated and glycosylated human fc gamma receptors. *Biotechnol Prog* 2024; **40**: e3392. https://doi.org/10.1002/btpr.3392.
39. Ramsland, PA, Farrugia, W, Bradford, TM. *et al.* Structural basis for FcγRIIa recognition of human IgG and formation of inflammatory Signaling complexes. *J Immunol* 2011; **187**: 3208–17. https://doi.org/10.4049/jimmunol.1101467.
40. Ferrara, C, Grau, S, Jäger, C. *et al.* Unique carbohydrate–carbohydrate interactions are required for high affinity binding between FcγRIII and antibodies lacking core fucose. *Proc National Acad Sci* 2011; **108**: 12669–74. https://doi.org/10.1073/pnas.1108455108.
41. Sondermann, P, Huber, R, Oosthuizen, V. *et al.* The 3.2-a crystal structure of the human IgG1 fc fragment-fc gammaRIII complex. *Nature* 2000; **406**: 267–73. https://doi.org/10.1038/35018508.
42. Shields, RL, Namenuk, AK, Hong, K. *et al.* High resolution mapping of the binding site on human IgG1 for FcγRI, FcγRII, FcγRIII, and FcRn and design of IgG1 variants with improved binding to the FcγR*. *J Biol Chem* 2001; **276**: 6591–604. https://doi.org/10.1074/jbc.M009483200.
43. Liu, Z, Gunasekaran, K, Wang, W. *et al.* Asymmetrical fc engineering greatly enhances antibody-dependent cellular cytotoxicity (ADCC) effector function and stability of the modified antibodies. *J Biol Chem* 2014; **289**: 3571–90. https://doi.org/10.1074/jbc.M113.513366.
44. Chen, C, Wang, Z, Sun, Z. *et al.* Development of an efficient method for selection of stable cell pools for protein expression and surface display with Expi293F cells. *Cell Biochem Funct* 2023; **41**: 355–64. https://doi.org/10.1002/cbf.3787.